Journal of Physical Science, Vol. 32(3), 61–73, 2021

Structural and Optical Properties of MAl_2O_4 Spinel-type Prepared by Solution Combustion Synthesis Method for Photocatalytic Application

Khaled Mahi[1,2*] and Rabah Mostefa[1]

[1]Department of Physics, Faculty of Sciences of the Matter, University of Tiaret, BP P 78 Zaaroura, Tiaret 14000, Algeria
[2]Laboratory of Plasma Physics, Conductor Materials and their Applications, Faculty of Physics, Oran University of Sciences and Technology - Mohamed Boudiaf USTO-MB, BP1505, Oran 31000, Algeria

[*]Corresponding author: khaled.mahi@univ-tiaret.dz

Published online: 25 November 2021

To cite this article: Mahi, K. & Mostefa, R. (2021). Structural and optical properties of MAI_2O_4 spinel-type prepared by solution combustion synthesis method for photocatalytic application. *J. Phys. Sci.*, 32(3), 61–73. https://doi.org/10.21315/jps2021.32.3.5

To link to this article: https://doi.org/10.21315/jps2021.32.3.5

ABSTRACT: *In this research, the aluminate spinel type materials, MAl_2O_4, are synthesised by solution combustion synthesis (SCS) method to investigate the effect of the element (M = Ca and Ba) on their structural, mainly crystallinity and optical properties. The characterisations are examined by X-ray diffraction (XRD), Fourier transform infrared spectroscopy (FT-IR) and UV-visible diffuse reflectance spectroscopy (UV-DRS). The XRD and FT-IR results showed the formation of the single-phase spinel structure of $CaAl_2O_4$ and $BaAl_2O_4$. The band gap energy was investigated using the Tauc method, and the obtained values were 3.93 eV and 3.77 eV for $CaAl_2O_4$ and $BaAl_2O_4$, respectively. The results showed a good agreement with the data as reported in the literature.*

Keywords: $CaAl_2O_4$, $BaAl_2O_4$, spinel oxides, photocatalysis, synthesis of powder

1. INTRODUCTION

Nanomaterials semiconductor-based photocatalysis have attracted attention, due to the absorbing quality and consequently, the use of visible light (to directly convert the solar energy), allowing environmental remediation to be implemented and solar fuels to be synthesised.

Several materials of semiconductors have been tested in photocatalytic processes.[1–6] The spinel-type oxides with the general formula MAl_2O_4, with M representing a divalent metal ion that has attracted considerable attention for diverse applications owing to its chemical stability, high mechanical resistance, large surface area and low surface acidity.[7,8] These unusual properties of spinel materials can be used in various areas of advanced technology. For example, it can be used in the military field to make missile domes, transparent armour, thermal camera windows and riflescope. It can also be used to make catalysts, luxury jewellery and horology, replacing sapphire and glass.[9–11] Researches revealed that the structural and optical properties of spinel oxides nanostructures can be controlled accurately by adjusting the chemical composition of the sample as well as changing the preparation method.[12,13]

Among the spinel-type structure compounds, aluminates, such as $CaAl_2O_4$ and $BaAl_2O_4$, seem to be good compounds to construct the hydrogen production catalysts.[14,15] These aluminates have high thermal and chemical stability, cation/anion vacancies and interesting luminescent properties, which can be used like refractory materials, capacitors, energy storage and recently they have been tested as catalysts due to their ability to generate hole/electron pairs during the oxidation/reduction reactions on the surface under light irradiation conditions.[16–18]

Recent research shows that the spinel aluminate (MAl_2O_4) nanopowders have astounding uses in several fields of applications. For the M element, calcium (Ca) and barium (Ba) are among the potential materials for various applications due to their flexibility, abundance and excellent electromagnetic performance.

Aluminium is a low-cost metal with high abundance, low toxicity and multiple valence bands. Moreover, aluminate has a high melting point (2135°C), low density (3.58 g/cm^3), excellent strength at extremely high temperatures and good resistance against chemical attacks.

In this work, we report the synthesis of MAl_2O_4 (M = Ca, Ba) spinel nanoparticles using the solution combustion synthesis (SCS) method. The characterisation of the prepared products is carried out using X-ray diffraction (XRD), Fourier transform infrared spectroscopy (FT-IR) and UV-visible diffuse reflectance spectroscopy (UV-DRS).

2. EXPERIMENTAL

2.1 Materials

The SCS is considered as an efficient, simple and economical synthetic method. It does not require any acid or base to hydrolyse the corresponding salts, and the steps of washing and filtration can be eliminated, which saves energy and time. The precursors used for the preparation of $CaAl_2O_4$ and $BaAl_2O_4$ were aluminium nitrate [$Al(NO_3)_3.9H_2O$ (Sigma Aldrich, purity 99.99%)], calcium [$Ca(NO_3)_2.4H_2O$ (Sigma Aldrich, purity 99.00%)], barium [$Ba(NO_3)_2$ (Sigma Aldrich, purity 99.00%)] and urea (CH_4N_2O) as the complexing agent that was very effective for the synthesis of our samples. All chemical reagents used were purchased from Sigma Aldrich (Darmstadt, Germany).

2.2 Sample Preparation and Characterisation Techniques

$CaAl_2O_4$ and $BaAl_2O_4$ were synthesised by SCS. We dissolved in 100 ml of distilled water, 10 g of $Al(NO_3)_3.9H_2O$ with 3.15 g of $Ca(NO_3)_2.4H_2O$ and 3.48 g of $Ba(NO_3)_2$, and 5 g of urea (CH_4N_2O) for both mixtures. The homogeneous solution obtained was placed under thermal agitation at 80°C, and after two h, a liquid was obtained. The formation of oxides ($CaAl_2O_4$ and $BaAl_2O_4$) by the combustion process is represented by the following chemical reactions:

$$6Al(NO_3)_3 + 3Ba(NO_3)_2 + 20NH_2CONH_2 \rightarrow 3BaAl_2O_4 + 20CO_2 + 32N_2 + 40H_2O$$

$$6Al(NO_3)_3 + 3Ca(NO_3)_2 + 20NH_2CONH_2 \rightarrow 3CaAl_2O_4 + 20CO_2 + 32N_2 + 40H_2O$$

To remove residual water, the gel was placed in an oven for 24 h at a temperature of 100°C. Finally, the as-synthesised powders were calcined in air at 900°C for 4 h. The solution combustion method was used to prepare the spinel type oxides (MAl_2O_4, M = Ca, Ba) in several steps as shown in Figure 1.

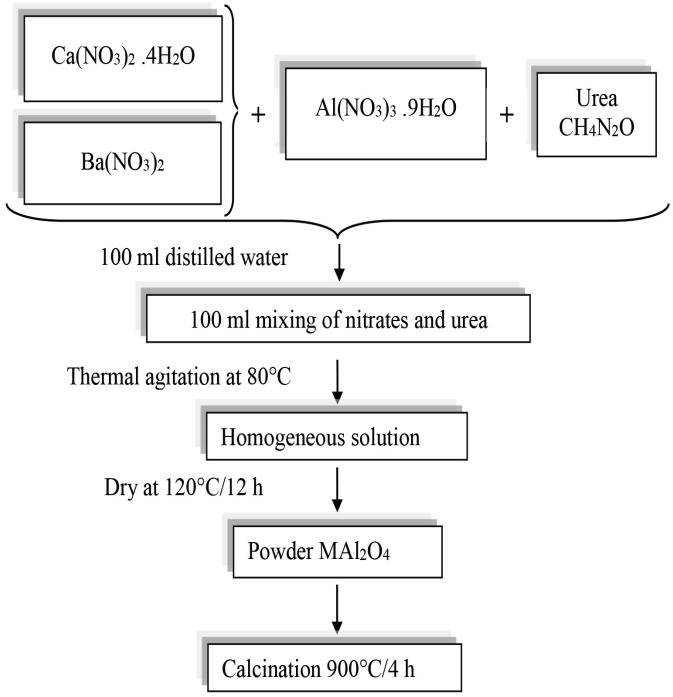

Figure 1: Flow chart for the synthesis of MAl_2O_4 powder by SCS method.

The effects of the element (M = Ca, Ba) on the structure such as crystallinity and optical properties of MAl_2O_4 were investigated by XRD, UV-DRS, and FT-IR.

3. RESULTS AND DISCUSSION

3.1 XRD Analysis

The XRD diagram was obtained using a PHILIPS PW 1800 powder diffractometer at the Synthesis and Catalysis Laboratory (University of Tiaret, Algeria). The radiations were used with a wavelength λ = 1.54056 A˚ produced by a copper anticathode. The interval explored in 2θ varied between 10° and 90° with a step of 0.02°.

Figures 2 and 3 show the XRD pattern of the $CaAl_2O_4$ and $BaAl_2O_4$ powders, respectively. We observed the presence of several well-defined lines. All the peaks correspond to the spinel phase of the $CaAl_2O_4$ and $BaAl_2O_4$ and are indexed in the base of the hexagonal crystal structure including the space group P63 N° 173, ICSD (Inorganic Crystal Structure Database).[17]

The presence of diffraction peaks at 2θ values, approximately equal to 19.00°, 21.95°, 23.95°, 26.98°, 30.14°, 31.40°, 33.34°, 35.70°, 37.44°, 41.11°, 42.30°, 44.76°, 74.42°, and 49.62° indexed to (112), (020), (211), (122), (220), (301), (311), (303), (313), (232), (323), (412), (420), and (414) planes for $CaAl_2O_4$ and 19.66°, 20.26°, 22.15°, 28.38°, 34.41°, 35.94°, 40.25°, 41.18°, 45.18°, 46.03°, 53.72°, 54.71°, 58.00°, 58.71°, 61.63°, 69.85°, 72.53°, 74.43°, 76.83°, 79.63°, and 87.98° indexed to (100), (002), (101), (102), (110), (111), (112), (004), (202), (104), (210), (114), (212), (204), (300), (214), (220), (116), (304), (312), and (216) planes for $BaAl_2O_4$ were confirmed by the JCPDS card No. 2002888 and JCPDS card No. 1010630, respectively.

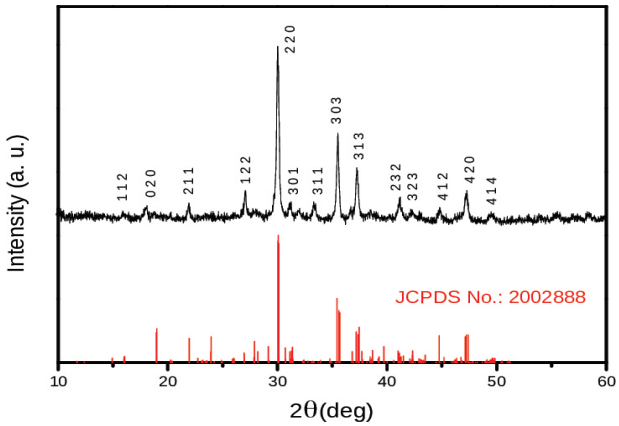

Figure 2: XRD patterns of $CaAl_2O_4$ powder compared with JCPDS PDF Card No. 2002888.

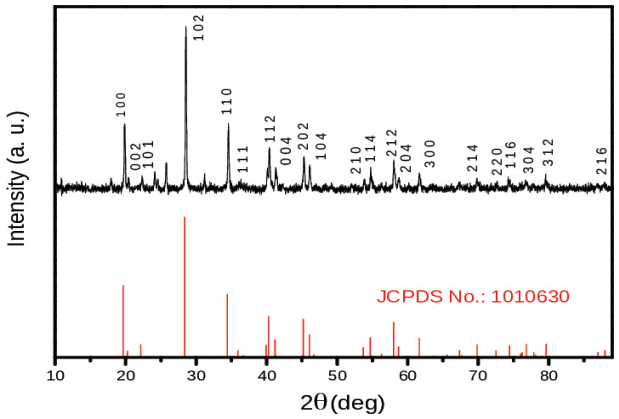

Figure 3: XRD patterns of $BaAl_2O_4$ powder compared with JCPDS PDF Card No. 1010630.

From the measurement XRD data we can calculate the crystallite size, the lattice constant and the cell volume.

To calculate the lattice parameter (a), the following expression is used:

$$a = \frac{\lambda}{2}\frac{(h^2 + k^2 + l^2)}{\sin\theta} \quad (1)$$

where λ is X-ray wavelength, hkl represents the Miller indices and θ denotes the diffraction angle corresponding to the hkl plane.

The unit volume (V) of the prepared aluminate spinels is calculated using the following expression:

$$V = \frac{\sqrt{3}}{2}a^2c \quad (2)$$

The crystallite size (D) of the samples is determined by the following Debye Scherer's equation:[19,20]

$$D = \frac{k\lambda}{\beta\cos\theta} \quad (3)$$

where k shows the crystallite shape factor, β is the half width maximum, and θ illustrates the Bragg's angle.

The results obtained for the lattice parameter (a) gave the crystallite size (D) and the cell volume (V) for both samples as listed in Table 1.

Table 1: Lattice constant (a), cell volume (V) and crystallite size (D) for both structures ($CaAl_2O_4$, $BaAl_2O_4$).

Sample	a = b(A°)		c (A°)		V(A°³)	D (nm)
	Exp	Th[1,22]	Exp	Th[21,22]		
$CaAl_2O_4$	08.71	08.70	8.09	8.71	530.45	26.0
$BaAl_2O_4$	10.42	10.45	8.78	8.78	825.58	34.6

Note: b and c = lattice parameter, Exp = experimental, Th = theoretical

The computations indicated the value of crystallite size, the cell volume, and the lattice constant that increased with the M element substitution. The lattice constant

enhancement is due to the difference in the ionic radii of both Ca and Ba. The cell volume and lattice constant rise is due to the inter-atomic distance among the particles increases.

3.2 FT-IR Spectroscopy Analysis

This analysis was performed to follow the chemical evolution of the powder during preparation, by detecting each atomic bond created or disappeared. The FT-IR spectra (400–4000 cm^{-1}) obtained for spinel powders ($CaAl_2O_4$ and $BaAl_2O_4$) are illustrated in Figures 4 and 5.

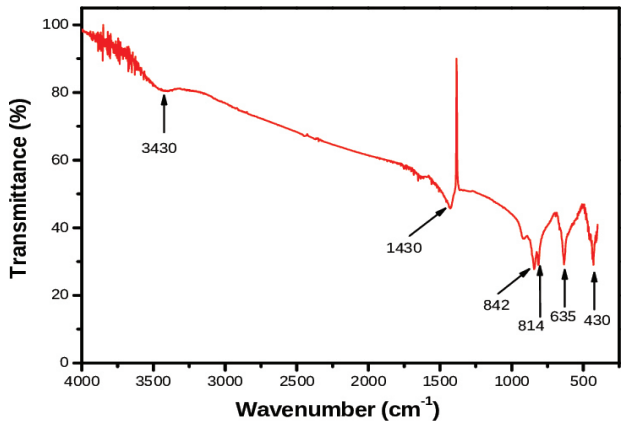

Figure 4: FT-IR spectra of $CaAl_2O_4$ powder synthesised via SCS method and calcined at 900°C for 4 h.

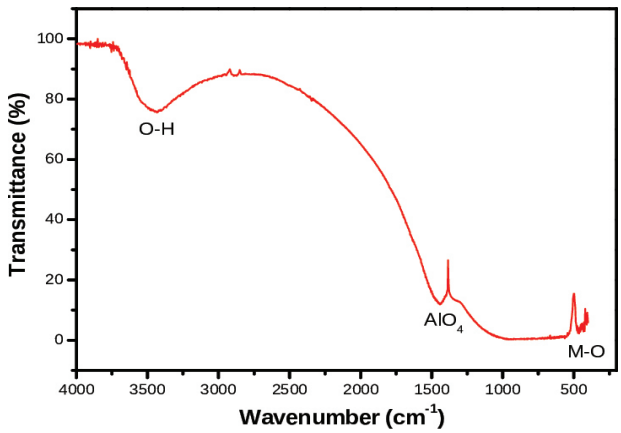

Figure 5: FT-IR spectra of $BaAl_2O_4$ powder synthesised via SCS method and calcined at 900°C for 4 h.

Both samples contain common absorption bands around 3460, 1430, and 430 cm^{-1}. The broad bands near 3460 cm^{-1} are attributed to O–H stretching vibrational and bending vibrational modes of absorbed water molecules.[23]

Some infrared (IR) investigations of aluminate spinels observed are due to water absorption peaks and express that the high surface area of these materials would result in rapid adsorption of water from the atmosphere during pellet compression and IR measurements.[23,24]

Additionally, the band at 1430 cm^{-1} is approved to the asymmetric stretching vibrations of AlO_4 for both samples. In the FT-IR spectrum of Figures 4 and 5, the bands present in the range 400–500 cm^{-1} correspond to sites of the Ca and Ba, respectively. These bands are frequently reported in this range for similar spinel aluminate.[25,26]

3.3 UV-DRS Analysis

UV-vis absorbance spectra for both structure $CaAl_2O_4$ and $BaAl_2O_4$ are shown in Figures 6 and 7, where it is observed that the materials could efficiently absorb energy below 310 nm, allowing them to be considered UV activated photocatalysts. Additionally, it is possible to observe an absorption peak between 350 and 450 nm for $CaAl_2O_4$ and $BaAl_2O_4$.

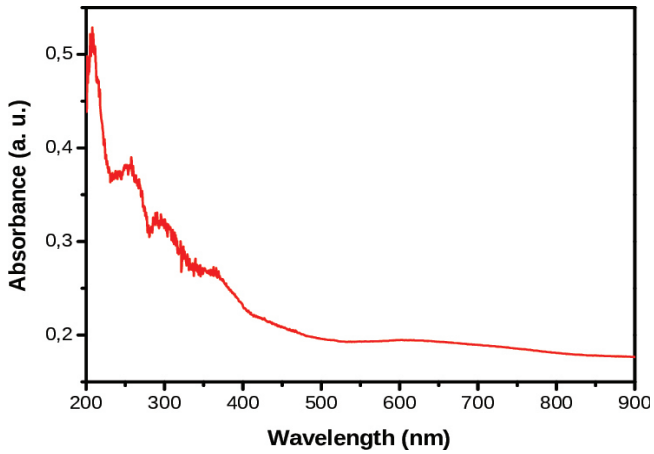

Figure 6: Absorbance plots of $CaAl_2O_4$ powder synthesised via SCS method and calcined at 900°C for 4 h.

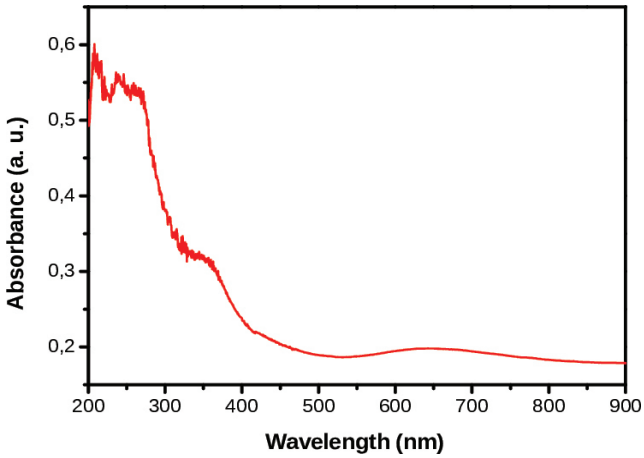

Figure 7: Absorbance plots of $BaAl_2O_4$ powder synthesised via SCS method and calcined at 900°C for 4 h.

The experimental band-gap values are evaluated from Tauc's graphs by extrapolating the linear portion of $(\alpha h\upsilon)^2$ for the band gap versus the photon energy:[27,28]

$$(\alpha h\upsilon)^n = A\,(h\upsilon - E_g) \tag{4}$$

where $h\upsilon$ is the light energy, A is a constant, E_g is the band gap energy, n = 1/2 for direct band gap.

Figures 8 and 9 display the curves of $(\alpha h\upsilon)^2$ versus $h\upsilon$ for $BaAl_2O_4$ and $CaAl_2O_4$ components synthesised. From these figures, the calculated band gap for $CaAl_2O_4$ and $BaAl_2O_4$ are 3.93 eV and 3.77 eV, respectively. These values can be compared with the band gap values cited in the literature.[29] This change in the value of the optical band gap (E_g) depends on several factors, such as the type of cation (Ca, Ba) introduced in the structure, preparation conditions, lattices train, and size effect.

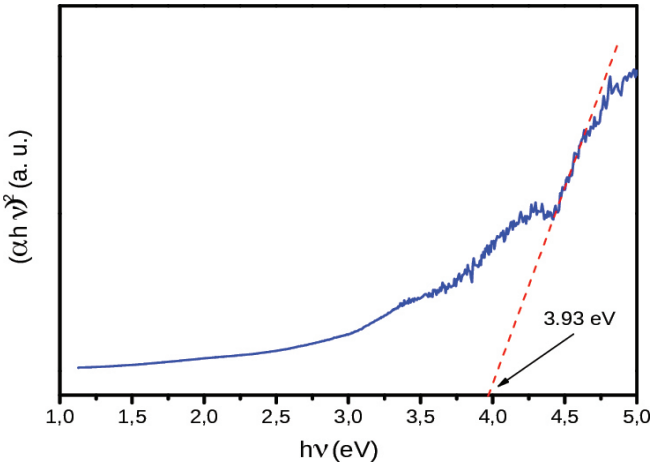

Figure 8: Tauc's plots of $CaAl_2O_4$ powder synthesised via SCS method and calcined at 900°C for 4 h.

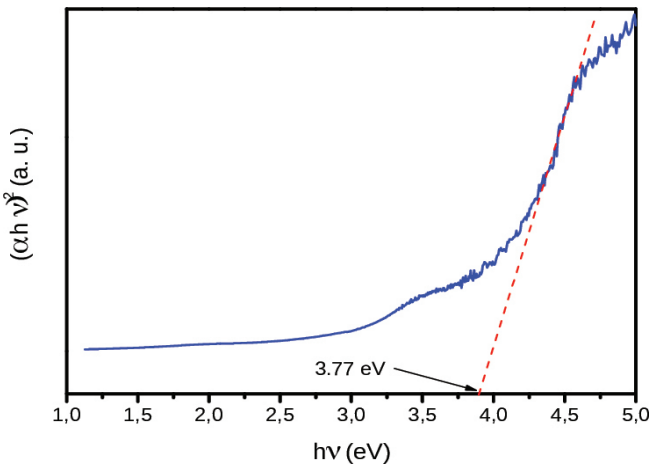

Figure 9: Tauc's plots of $BaAl_2O_4$ powder synthesised via SCS method and calcined at 900°C for 4 h.

4. CONCLUSION

The nanopowders of the aluminate-based spinels (MAl_2O_4, M = Ca, Ba) synthesised in this work were successfully obtained by SCS method. XRD results proved that the spinel phase was for both samples with no secondary phase. An important difference in the lattice parameter (a), the cell volume (V) and the crystalline size (D) was observed. The formation of a spinel structure was confirmed by

the FT-IR spectroscopy absorption bands in the 400–500 cm^{-1} frequency range. The change in the band gap values determined by Tauc relation, elucidated the absorption wavelength variation of spinel aluminates according to the M element. Based on the investigations of all properties, it is concluded that the synthesised spinel aluminates are efficient constituents used as catalysts. Moreover, the SCS method can be considered as a very effective and useful technique to synthesise other spinel-type oxides aluminate nanopowders with good structural and optical properties.

5. ACKNOWLEDGEMENTS

The authors thank the Engineering Physics Laboratory and the Synthesis and Catalysis Laboratory of University of Tiaret, Algeria for their help in XRD, FT-IR and UV-visible measurements. Furthermore, the authors would like to thank Professor Djamel Turki (University Ibn-Khaldoun, Tiaret, Algeria) for English language proofreading and review. This work was financed by the Faculty of Sciences of the Matter, University Ibn-Khaldoun, Tiaret, Algeria (grant No. 39329/FSM.UT/D.11/2019).

6. REFERENCES

1. Chen, P. F. et al. (2020). Microwave heating preparation of phosphorus doped g-C_3N_4 and its enhanced performance for photocatalytic H_2 evolution in the help of Ag_3PO_4 nanoparticles. *Int. J. Hydrog. Energy*, 45(28), 14354–14367. https://doi.org/10.1016/j.ijhydene.2020.03.169
2. Singh, R. & Dutt, S. (2018). A review on H_2 production through photocatalytic reactions using TiO_2/TiO_2-assisted catalysts. *Fuel*, 220(19), 607–620. https://doi.org/10.1016/j.fuel.2018.02.068
3. Ong, C. B., Ng, L. Y. & Mohammad, A. W. (2018). A review of ZnO nanoparticles as solar photocatalysts: Synthesis, mechanisms and applications. *Renew Sustain. Energy Rev*., 81(P1), 536–551. https://doi.org/10.1016/j.rser.2017.08.020
4. Wang, X. C. et al. (2009). A metal-free polymeric photocatalyst for hydrogen production from water under visible light. *Nat Mater*., 8(1), 76–80. https://doi.org/10.1038/nmat2317
5. Zong, X. et al. (2008). Enhancement of photocatalytic H_2 evolution on CdS by loading MoS_2 as cocatalyst under visible light irradiation. *J. Am. Chem. Soc*., 130(23), 7176–7177. https://doi.org/10.1021/ja8007825
6. Feng, Z. et al. (2020). In situ preparation of g-C_3N_4/$Bi_4O_5I_2$ complex and its elevated photoactivity in Methyl Orange degradation under visible light. *J. Environ. Sci.*, 87(1), 149–162. https://doi.org/10.1016/j.jes.2019.05.032

7. Sharma, R. K. & Ghose, R. (2014). Synthesis and characterization of nanocrystalline zinc aluminate spinel powder by sol-gel method. *Ceram. Int.*, 40(2), 3209–3214. https://doi.org/10.1016/j.ceramint.2013.09.121
8. Ravikumar, B. S. et al. (2015). *Calotropis procera* mediated combustion synthesis of $ZnAl_2O_4$: Cr^{3+} nanophosphors: Structural and luminescence studies. *Spectrochim. Acta A Mol Biomol. Spectrosc.*, 136(Part B), 1027–1037. https://doi.org/10.1016/j.saa.2014.09.126
9. Stringhini, F. M. et al. (2014). Synthesis of porous zinc aluminate spinel ($ZnAl_2O_4$) by metal-chitosan complexation method. *J. Alloys Compd*., 588(3), 305–309. https://doi.org/10.1016/j.jallcom.2013.11.078
10. Davar, F. & Salavati-Niasari, M. (2011). Synthesis and characterization of spinel-type zinc aluminate nanoparticles by a modified sol-gel method using new precursor. *J. Alloys Compd*., 509(5), 2487–2492. https://doi.org/10.1016/j.jallcom.2010.11.058
11. Quirino, M. R. et al. (2016). Synthesis of zinc aluminate with high surface area by microwave hydrothermal method applied in the transesterification of soybean oil (biodiesel). *Mater. Res. Bull*., 74(2), 124–128. https://doi.org/10.1016/j.materresbull.2015.10.027
12. Kumar, K. V., Paramesh, D. & Reddy, P. V. (2015). Effect of aluminium doping on structural and magnetic properties of Ni-Zn ferrite nanoparticles. *World J. Nano. Sci. Eng.*, 5(3), 68–77. https://doi.org/10.4236/wjnse.2015.53009
13. Gul, I. H. & Pervaiz, E. (2012). Comparative study of $NiFe_{2-x}Al_xO_4$ ferrite nanoparticles synthesized by chemical co-precipitation and sol–gel combustion techniques. *Mater. Res. Bull.*, 47(6), 1353–1361. https://doi.org/10.1016/j.materresbull.2012.03.005
14. Wako, A. H. Dejene, F. B. & Swart, H. C. (2014). Combustion synthesis, characterization and luminescence properties of barium aluminate phosphor. *J. Rare Earths*, 32(9), 806–811. https://doi.org/10.1016/S1002-0721(14)60145-9
15. Mothudi, B. M. et al. (2009). Photoluminescence and phosphorescence properties of MAl_2O_4: Eu^{2+}, Dy^{3+} (M = Ca, Ba, Sr) phosphors prepared at an initiating combustion temperature of 500°C. *Physica B Condens. Matter*, 404(22), 4440–4444. https://doi.org/10.1016/j.physb.2009.09.047
16. Zhang, L. W., Wang, L. & Zhu, Y. F. (2007). Synthesis and performance of $BaAl_2O_4$ with a wide spectral range of optical absorption. *Adv. Funct. Mater*., 17(18), 3781–3790. https://doi.org/10.1002/adfm.200700506
17. Nassar, M. Y. Ahmed, I. S. & Samir, I. (2014). A novel synthetic route for magnesium aluminate ($MgAl_2O_4$) nanoparticles using sol-gel auto combustion method and their photocatalytic properties. *Spectrochim. Acta A Mol. Biomol. Spectrosc.*, 131(10), 329–334. https://doi.org/10.1016/j.saa.2014.04.040
18. Lv, W. et al. (2009). Synthesis, characterization and photocatalytic properties of spinel $CuAl_2O_4$ nanoparticles by a sonochemical method. *J. Alloys Compd*., 479 (1–2), 480–483. https://doi.org/10.1016/j.jallcom.2008.12.111
19. Klug, H. P. & Alexander, L. E. (1974). *X-ray diffraction procedures: For polycrystalline and amorphous materials*, 2nd ed. New York: John Wiley and Sons.

20. Salavati-Niasari, M., Davar, F. & Mahmoudi, T. (2009). A simple route to synthesize nanocrystalline nickel ferrite ($NiFe_2O_4$) in the presence of octanoic acid as a surfactant. *Polyhedron*, 28(8), 1455–1458. https://doi.org/10.1016/j.poly.2009.03.020
21. Singh, V. et al. (2007). Synthesis, characterisation and luminescence investigations of Eu activated $CaAl_2O_4$ phosphor. *Opt. Mater.*, 30(3), 446–450. https://doi.org/10.1016/j.optmat.2006.11.074
22. Ianos, R. et al. (2013). Nanocrystalline $BaAl_2O_4$ powders prepared by aqueous combustion synthesis. *Ceram. Int*., 39(3), 2645–2650. https://doi.org/10.1016/j.ceramint.2012.09.030
23. Ge, D. L. et al. (2013). Facile synthesis of highly thermostable mesoporous $ZnAl_2O_4$ with adjustable pore size. *J. Mater. Chem. A*, 1(5), 1651–1658. https://doi.org/10.1039/c2ta00903j
24. Wei, X. H. & Chen, D. H. (2006). Synthesis and characterization of nanosized zinc aluminate spinel by sol-gel technique. *Mater. Lett.*, 60(6), 823–827. https://doi.org/10.1016/j.matlet.2005.10.024
25. Baig, M. M. et al. (2019). Optimization of different wet chemical routes and phase evolution studies of $MnFe_2O_4$ nanoparticles. *Ceram. Int*., 45(10), 12682–12690. https://doi.org/10.1016/j.ceramint.2019.03.114
26. Yousuf, M. A. et al. (2019). The impact of yttrium cations (Y^{3+}) on structural, spectral and dielectric properties of spinel manganese ferrite nanoparticles. *Ceram. Int.*, 45(8), 10936–10942. https://doi.org/10.1016/j.ceramint.2019.02.174
27. Salavati-Niasari, M., Ghanbari, D. & Loghman-Estarki, M. R. (2012). Star-shaped PbS nanocrystals prepared by hydrothermal process in the presence of thioglycolic acid. *Polyhedron*, 35(1), 149–153. https://doi.org/10.1016/j.poly.2012.01.010
28. Mortazavi-Derazkola, S. et al. (2017). Fabrication and characterization of Fe_3O_4@SiO_2@TiO_2@Ho nanostructures as a novel and highly efficient photocatalyst for degradation of organic pollution. *J. Energy Chem.*, 26(1), 17–23. https://doi.org/10.1016/j.jechem.2016.10.015
29. Salehabadi, A. et al. (2017). Sol-Gel auto-combustion synthesis and physicochemical properties of $BaAl_2O_4$ nanoparticles; electrochemical hydrogen storage performance and density functional theory. *Renew. Energy*, 114(Part B), 1419–1426. https://doi.org/10.1016/j.renene.2017.07.119